conditions. Such a study has been initiated by the authors inspired by the present results.

The future role of computations in such optimizations is to address issues where experiments are limited. For example, consider the optimization of the physical shape of realistic actuators. It would be difficult to design hardware with the flexibility to provide a general shape for the actuation. However, in a simulation, it is straightforward to implement actuators of nearly any shape, and they may be constrained so that determined optimal geometry is realizable in hardware. This way the final configuration can be built and applied.

References

[1]Rechenberg, I., *Evolutionsstrategie: Optimierung Technischer System nach Prinzipien der biologischen Evolution*, Fromman–Holzboog, Stuttgart, Germany, 1973, pp. 1–170.

[2]Michalewicz, Z., *Genetic Algorithms + Data Structures + Evolution Programs*, Springer-Verlag, Berlin, 1996, pp. 1–387.

[3]Schwefel, H.-P., *Evolution and Optimum Seeking*, Wiley, New York, 1995, pp. 105–118.

[4]Freund, J. B., and Moin, P., "Jet Mixing Enhancement by High-Amplitude Fluidic Actuation," *AIAA Journal*, Vol. 38, No. 10, 2000, pp. 1863–1870.

[5]Parekh, D. E., Kibens, V., Glezer, A., Wiltse, J. M., and Smith, D. M., "Innovative Jet Flow Control: Mixing Enhancement Experiments," AIAA Paper 96-0308, 1996.

[6]Lee, M., and Reynolds, W. C., "Bifurcating and Blooming Jets," Dept. of Mechanical Engineering, Rept. TF-22, Stanford Univ., Stanford, CA, Aug. 1995.

[7]Parekh, D., Leonard, A., and Reynolds, W. C., "Bifurcating Jets at High Reynolds Numbers," Dept. of Mechanical Engineering, Rept. TF-35, Stanford Univ., Stanford, CA, Dec. 1988.

[8]Hilgers, A., "Parameter Optimization in Jet Flow Control," Center for Turbulence Research Annual Research Brief, Center for Turbulence Research, Stanford Univ., Stanford, CA, 1999, pp. 179–194.

J. P. Gore
Associate Editor

General Attenuation Laws for Spherical Shock Waves in Pure and Dusty Gases

F. Aizik,* G. Ben-Dor,† T. Elperin,† and O. Igra†
Ben-Gurion University of the Negev, 84105 Beer Sheva, Israel

Introduction

THE most common shock wave in nature is a spherical one. This is the reason for the importance of knowing the flowfield that is developed behind a spherical shock wave. The full governing equations that describe the flowfield consist of nonlinear partial differential equations. Because of their complexity and unless simplifying assumptions are applied, they can be solved only numerically. The numerical solution requires significant resources (time, computers, etc.). The complexity of solving these equations on one hand, and the importance, in many applications, of knowing the flowfield properties in real time, on the other hand, was our motivation to develop an alternative way of obtaining the flowfield properties immediately behind the shock wave front.

Olim et al.,[1] in their study of the flowfield that is developed behind attenuating planar shock waves propagating in a dusty air, showed that the numerical simulation could be replaced by a semi-empirical relation describing the instantaneous shock wave Mach number, that is, the shock wave velocity divided by the speed of sound of the gaseous phase ahead of it.

The correlation proposed by Ref. 1 implied that the shock wave degenerated to a sound wave, that is, $M_s \to 1$, when $x \to \infty$ as, indeed, should the case be if the wave is unsupported. However, Sommerfeld[2] found in the course of his experimental investigation, which was conducted in a shock tube in a finite length domain, that if the initial shock wave was strong and the dust-loading ratio was low to moderate, the shock wave did not attenuate to a sound wave but to a finite strength shock wave whose Mach number was larger than unity.

Because of this observation, Aizik et al.[3] modified the attenuation law suggested in Ref. 1. Kurian and Das[4] recently reported good agreement when they compared predictions based on the modified attenuation law of Ref. 3 with their experimental results.

The purpose of the present study was to extend the studies just mentioned and develop two general attenuation laws for spherical shock waves propagating 1) in pure gases and 2) in particle-laden gases.

Present Study

Rupturing a spherical diaphragm inside which the pressure p_4 was higher than the ambient pressure p_1 and the temperature T_4 was higher or equal to the ambient temperature T_1 generated the spherical shock wave. The particles, in the gas–particle suspension case, were uniformly distributed outside the spherical diaphragm.

The governing equations describing the propagation of a spherical shock wave through both pure and particle-laden gases were formulated and solved numerically using the random choice method (RCM) with operator splitting technique.

The computer code was validated by comparing its predictions to all of the experimental results of Boyer.[5,6] Very good agreement was evident. Full details of the comparison can be found in Ref. 7, where a detailed derivation of the governing equations and their final form are also given. The assumptions on which the governing equations were based were as follows: 1) The flowfield is one-dimensional (radial) and unsteady. 2) The gaseous phase behaves as a perfect gas. 3) The solid particles, which are identical in all their physical properties, are rigid spherical and inert. They are uniformly distributed in the gaseous phase. 4) The number density of the solid particles is sufficiently high for considering the solid phase as a continuous medium. 5) The solid particles do not interact with each other. As a result, their partial pressure in the suspension is negligibly small. 6) The volume occupied by be solid particles is negligibly small. 7) The heat capacity of the solid particles is constant. 8) The dynamic viscosity, the thermal conductivity, and the specific heat capacity at constant pressure of the gaseous phase depend solely on its temperature. 9) Other than the momentum and energy exchanges between the solid and the gaseous phases, the gaseous phase is assumed to be an ideal fluid, that is, inviscid and thermally nonconductive. 10) The weight of the solid particles and the buoyancy force are negligibly small compared to the drag force acting on them. 11) The solid particles are too large to experience a Brownian motion. 12) The temperature within the solid particles is uniform.

General Attenuation Law of Spherical Shock Waves Propagating in Pure Gases

The governing equations were solved numerically for a variety of initial conditions, to identify the parameters affecting the spherical shock wave attenuation. As expected, in the case of a pure gas, the most dominant parameter was its initial strength, that is, the initial Mach number, which can be derived from the pressure and the temperature ratios ($P_{41} = p_4/p_1$ and $T_{41} = T_4/T_1$, respectively) across the spherical diaphragm (e.g., see Ref. 8).

The numerical results indicated that an exponential curve could well fit the primary spherical shock wave attenuation. In addition, it is well known that spherical shock waves degenerate to sound waves far away from their origin. Under this constraint the spherical shock wave attenuation was described by

$$M_s = (M_{s,0} - 1)\exp[-(r - r_0)/\Re] + 1 \qquad (1)$$

Received 26 October 1999; revision received 20 October 2000; accepted for publication 20 December 2000.

*Graduate Student, Department of Mechanical Engineering.

†Professor, Pearlstone Center for Aeronautical Engineering Studies, Department of Mechanical Engineering.

where M_s is the instantaneous shock wave Mach number at the radius r, $M_{s,0}$ is the initial shock wave Mach number, $\Re$ is the decay coefficient, and r_0 is the radius of the diaphragm. Correlation (1) describes appropriately the exponential nature of the spherical shock wave attenuation and it fulfills the following boundary conditions:

$$M_s = \begin{cases} M_{s,0} & \text{for} \quad r = r_0 \\ 1 & \text{for} \quad r = \infty \end{cases}$$

The decay coefficient $\Re$ depends on the initial strength of the spherical shock wave $M_{s,0}$, the temperatures ratio of the confined gas inside the diaphragm before its rupture, and the ambient gas T_{41}.

The governing equations were solved for the following range of parameters: $1.1 < M_{s,0} < 5$ and $1 < T_{41} < 6$. The upper values were limited by the assumption that the gas behaved as a perfect gas. The decay coefficient $\Re$ was obtain by a curve fitting analysis of the numerical results to Eq. (1) for 90 combinations of initial conditions in the following form:

$$\Re(M_{s,0}, T_{41}) = (C_1 + C_2 \cdot T_{41}) \cdot M_{s,0} \tag{2}$$

Substituting Eq. (2) into Eq. (1) results in the following expression for the attenuation of spherical shock waves, generated from finite sources, in a pure gas:

$$M_s = (M_{s,0} - 1) \exp\left[-\frac{r - r_0}{(C_1 + C_2 T_{41})\, M_{s,0}} \right] + 1 \tag{3}$$

where $C_1 = 1.48044$ m and $C_2 = -0.10839$ m.

The general attenuation law (3) enables one to calculate the instantaneous spherical shock wave Mach number within 97% accuracy, without the need to conduct any complicated numerical calculations. The general attenuation law (3) was validated by comparing its predictions to the experimental results of Ref. 6. A typical comparison is shown in Fig. 1. The agreement between the predicted attenuation and the actual (experimental) attenuation is very good. Here $\lambda_s = r/r_0$ is the nondimensional distance.

Additional comparisons were made between the predicted attenuation and the results of full numerical solutions of the governing equations. Two typical comparisons are shown in Figs. 2a and 2b. Again, the agreement is very good. Note that it is better for stronger initial shock waves. Again $\lambda_s = r/r_0$ is the nondimensional distance.

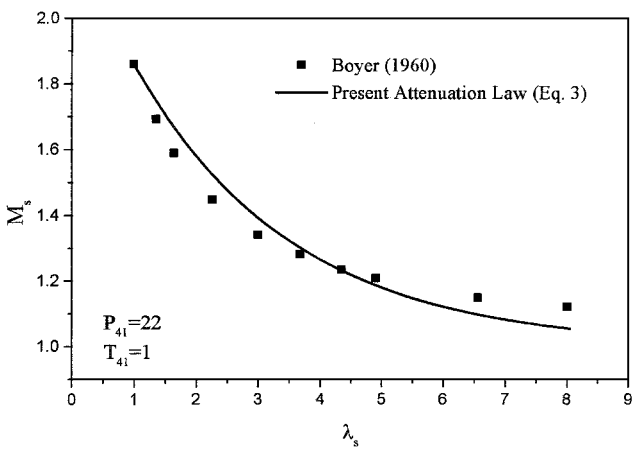

Fig. 1 Comparison between the primary spherical shock wave attenuation as predicted by the present attenuation law [Eq. (3)] (——) and the experimental results of Ref. 6 for an explosion of a 2-in.-diam sphere of pressurized air initially at 22 atm and room temperature.

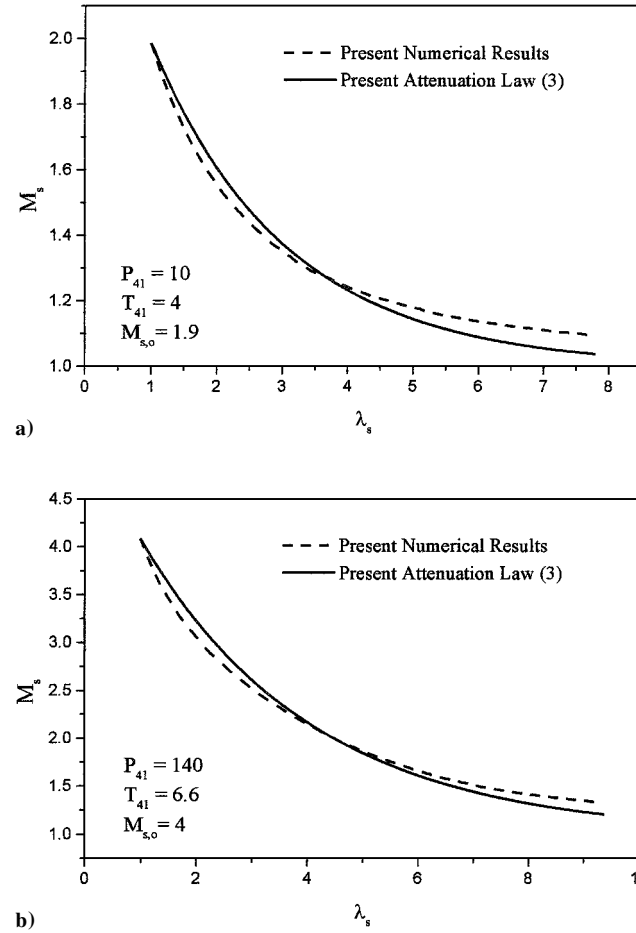

Fig. 2 Comparison between the primary spherical shock wave attenuation as predicted by the present attenuation law [Eq. (3)] (——) and the results obtained by full numerical solutions of the governing equations (– – –) for two cases: a) moderate initial shock wave and b) relatively strong initial shock wave.

General Attenuation Law of Spherical Shock Waves Propagating in Inert Gas–Particle Suspensions

The governing equations describing the flowfield developed behind a spherical shock wave propagating in an inert gas–particle suspension were formulated and solved numerically by using the random choice method with operator splitting technique (for more details see Ref. 7).

The governing equations were solved for $10 < P_{41} < 160$, $1 < T_{41} < 6$, $25 < D < 500$ μm and $0.25 < \eta < 10$. The density of the solid particles was kept constant in all of the calculations at 2500 kg/m^3. Note that the ranges assigned for P_{41} and T_{41} yield initial shock wave Mach numbers in the range $1.5 < M_{s,0} < 4$. The upper limit of the initial shock wave Mach number value, $M_{s,0}$, is dictated by the assumption that the gas behaves as a perfect gas. The diameter D is limited from above by assumptions 10 and 12 and from below by assumption 11. The highest loading ratio value η is limited by assumption 6. To quantify the latter, the volume of the solid particles was limited to a maximum of 1% of the suspension volume. All of the 480 ($4 \times 5 \times 4 \times 6$) possible combinations of the following values of the mentioned four parameters were used as initial conditions for the numerical investigation undertaken during the course of this part of the study: $D = 25$, 50, 100, and 500 μm; $\eta = 0.25$, 0.75, 2.0, 6.0, and 10.0; $P_{41} = 10$, 40, 80, and 160; and $T_{41} = 1$, 2, 3, 4, 5, and 6.

From the same considerations, as in the case of the pure gas, it was decided to describe the attenuation of the primary spherical shock wave propagating through gas–particle suspension by Eq. (1). However, unlike in the dust-free case, in the present case the decay coefficient $\Re$ depended also on the preshock suspension properties (the particle diameter D and the dust loading ratio $\eta = \rho_p/\rho_g$, where

ρ_p and ρ_g are the spatial densities of the solid and the gaseous phases, respectively) in addition to the dependence on the initial shock wave Mach number $M_{s,0}$ and the gas temperatures ratio T_{41}.

The first step was to obtain the decay coefficients $\mathfrak{R}$, for all of the 480 cases. This was done by applying a curve fitting analysis of the numerical results to Eq. (1). The following steps were to find the functional dependence of the decay coefficient $\mathfrak{R}$, which is a free parameter in Eq. (1), on $M_{s,0}$, D, and η. Details may be found in Ref. 7. The analysis resulted in

$$\mathfrak{R} = a_1 \exp(-a_5 \eta) \tag{4}$$

where

$$a_i = (c_i + c_{i+1} M_{s,0}) D^{(c_{i+2} + c_{i+3} M_{s,0})}, \qquad c_i = f(T_{41})$$

In Eq. (4) D should be inserted in micrometers to obtain $\mathfrak{R}$ in meters.

Substituting Eq. (4) into Eq. (1) gives the following general expression for the attenuation of a primary spherical shock wave, generated from a finite source, in an inert gas–particle suspension:

$$M_s = (M_{s,0} - 1) \exp\Big\{ -(r - r_0)/(c_1 + c_2 M_{s,0}) D^{(C_3 + C_4 M_{s,0})} \times \exp\big[-(c_5 + c_6 M_{s,0}) \eta D^{(C_7 + C_8 M_{s,0})}\big]\Big\} + 1 \tag{5}$$

where D should be inserted in micrometers and r_0 in meters. The values of c_i that ensure a 97% correlation of the curve fits with the numerical data are

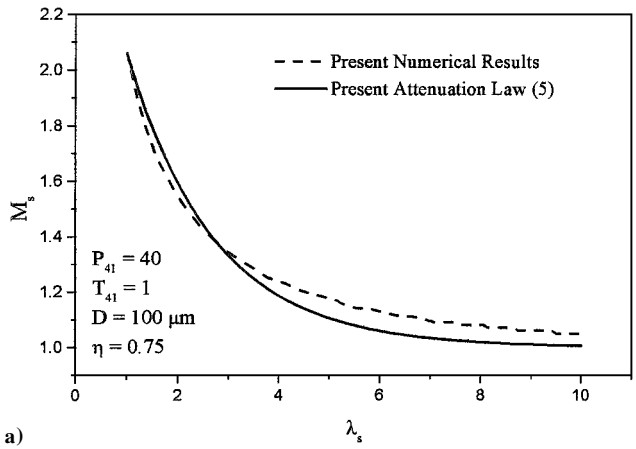

a)

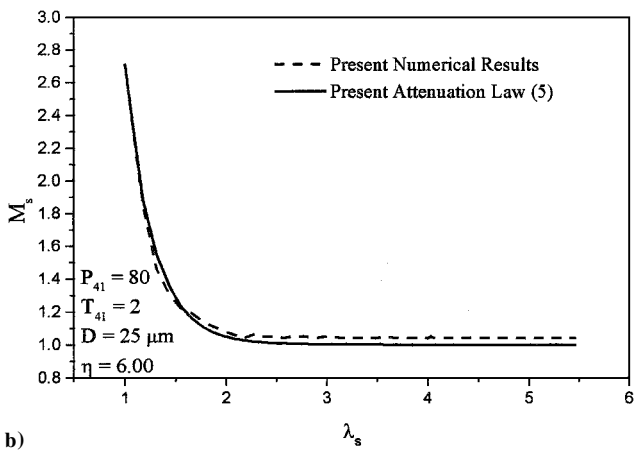

b)

Fig. 3 Comparison between the primary spherical shock wave attenuation as predicted by the present attenuation law [Eq. (5)] (——) and the results obtained by full numerical solutions of the governing equations for the same initial conditions (– – –) for two typical cases.

$$c_1 = 0.465 - 3.6557 \exp(-T_{41}), \qquad c_2 = 1.0586\, T_{41}^{-0.8268}$$

$$c_3 = 0.2650\, T_{41}^{-0.3003}, \qquad c_4 = -0.187 \exp(-T_{41})$$

$$c_5 = 34.168 - 0.2061\, T_{41}, \qquad c_6 = -11.6309 + 0.6442\, T_{41}$$

$$c_7 = -1.1177 - 0.0975\, T_{41}, \qquad c_8 = 0.1930 + 0.0298\, T_{41}$$

The general attenuation law given by Eq. (5) contains all of the flow parameters and dust physical properties that are known to affect the shock wave attenuation, namely, the initial shock wave Mach number $M_{s,0}$, the temperature ratio across the diaphragm, T_{41}, the dust loading ratio η, and its diameter D.

The general attenuation law enables one to calculate the instantaneous shock wave Mach number within 90% accuracy. As a result, the jump conditions across the attenuating shock wave front could be readily obtained without the need to numerically solve the entire flowfield.

Because, to the best of the authors' knowledge, experimental results similar to the investigated flowfield are not available, the prediction of the general attenuation law (5) could not be compared to experimental results. Instead, they were validated by comparing them to the full numerical solutions of the governing equations. Two such comparisons are shown in Figs. 3a and 3b. Very good agreement is evident. Again $\lambda_s = r/r_0$ is the nondimensional distance.

Conclusions

The governing equations describing the flowfields that develop when spherical shock waves, generated from a finite source, propagate inside pure and particle-laden gases were solved numerically using the RCM with operator splitting technique.

The attenuation of the primary shock wave was investigated numerically. Based on the numerical results, two general attenuation laws, for describing the primary shock wave attenuation as it propagates inside pure and particle-laden gases, were developed.

The general attenuation laws were validated by comparing their predictions to actual experimental results in the pure-gas case and to the results of full numerical solutions of the governing equations for the same initial conditions. Very good agreements were evident.

The general attenuation laws enables one to calculate simply and cheaply the instantaneous primary shock wave Mach number and as a result to readily obtain the jump conditions across it, without the need to conduct tedious full numerical simulations.

References

[1]Olim, M., Ben-Dor, G., Mond, M., and Igra, O., "A General Attenuation Law of Moderate Planar Shock Waves Propagating into Dusty Gases With Relatively High Loading Ratios of Solid Particles," *Fluid Dynamics Research*, Vol. 6, Nos. 3–4, 1990, pp. 185–200.

[2]Sommerfeld, M., "The Unsteadiness of Shock Waves Propagating through Gas–Particle Mixtures," *Experiments in Fluids*, Vol. 3, 1985, pp. 197–206.

[3]Aizik, F., Ben-Dor, G., Elperin, T., Igra, O., Mond, M., and Gronig, H., "Attenuation Law of Planar Shock Waves Propagating Through Dust Gas Suspensions," *AIAA Journal*, Vol. 33, No. 5, 1995, pp. 953–955.

[4]Kurian, J., and Das, H. K., "Studies of Shock Wave Propagation in Gas–Particle Mixtures," *Shock Waves*, edited by A. P. F. Houwing and A. Paull, Vol. 2, Panther, Sydney, Australia, 1997, pp. 953–958.

[5]Boyer, D.W., "Spherical Explosions and Implosions," Inst. of Aerophysics, Univ. of Toronto, UTIA Rept. 58, Toronto, ON, Canada, 1959.

[6]Boyer, D.W., "An Experimental Study of the Explosion Generated by a Pressurized Sphere," *Journal of Fluid Mechanics*, Vol. 9, Pt. 3, 1960, pp. 401–429.

[7]Aizik, F., "Investigation of Spherical Shock Waves Propagation in Inert and Reactive Gas-Particle Suspensions," Ph.D. Dissertation, Dept. of Mechanical Engineering, Ben-Gurion Univ. of the Negev, Beer Sheva, Israel, 1999 (in Hebrew).

[8]Emanuel, G., *Gasdynamics: Theory and Applications*, AIAA Education Series, AIAA, New York, 1986, p. 183.

M. Sichel
Associate Editor